

Inelastic neutron scattering and lattice-dynamics studies of almandine $\text{Fe}_3\text{Al}_2\text{Si}_3\text{O}_{12}$

R. Mittal, S. L. Chaplot, and N. Choudhury

Solid State Physics Division, Bhabha Atomic Research Centre, Trombay, Mumbai 400 085, India

C.-K. Loong

Intense Pulsed Neutron Source Division, Argonne National Laboratory, Argonne, Illinois 60439

(Received 4 August 1999)

This paper reports detailed lattice dynamical studies involving experimental inelastic neutron-scattering measurements and theoretical shell model calculations of the vibrational and thermodynamic properties of the garnet mineral almandine $\text{Fe}_3\text{Al}_2\text{Si}_3\text{O}_{12}$. Inelastic neutron-scattering studies using the time-of-flight technique provide the measurement of the phonon density of states (DOS) of almandine, which have been interpreted based on the model calculations. The calculated DOS is in good agreement with the inelastic neutron-scattering data and has been used to compute various macroscopic properties like the specific heat, thermal expansion, equation of state, and mean-square atomic displacements.

I. INTRODUCTION

Garnets with general formula $A_3B_2C_3O_{12}$ (where A , B , C are cations) are used in several devices including computer memories, lasers, and microwave optical elements.¹ The garnet minerals belong to an important group of rock-forming silicates, which are important constituents of the earth's crust, upper mantle, and transition zone. They are distinguished by their chemical diversity, close structural similarities, physical properties, and petrologic implications. Garnets are cubic (space group $Ia\bar{3}d$, $a = 11.5\text{--}12 \text{ \AA}$) and possess relatively high refractive index ($n = 1.7\text{--}1.94$), densities ($\rho = 3.5\text{--}4.3 \text{ gm/cm}^3$)¹ and hardness (6.5–7.5 mhos). Garnets are hosts for aluminum in the earth's upper mantle^{2,3} and at high pressures, transform to silicate perovskite,^{3–5} a predominant constituent of the earth's lower mantle. Rare-earth containing garnets exhibit a rich variety of colors across the visible spectrum, which makes them useful as gemstones.

The six ideal end-member garnets are pyrope $\text{Mg}_3\text{Al}_2\text{Si}_3\text{O}_{12}$, almandine $\text{Fe}_3\text{Al}_2\text{Si}_3\text{O}_{12}$, spessartine $\text{Mn}_3\text{Al}_2\text{Si}_3\text{O}_{12}$, uvarovite $\text{Ca}_3\text{Cr}_2\text{Si}_3\text{O}_{12}$, grossular $\text{Ca}_3\text{Al}_2\text{Si}_3\text{O}_{12}$, and andradite $\text{Ca}_3\text{Fe}_2\text{Si}_3\text{O}_{12}$. Because their cation composition changes continuously, the knowledge of their mixing properties is essential to the understanding of the chemistry involving garnets and rock substances. Accurate characterization of the structural, vibrational, and thermodynamic properties of constituent end-members phases are therefore very important.

X-ray diffraction,^{6,7} infrared, and Raman spectroscopy,⁸ ultrasonic^{9,10} and calorimetric studies^{11,12} have been used to understand the crystal structure, phonon frequencies, elastic constants, compressibilities, specific heat, and thermal expansion of several end member garnets. Inelastic neutron-scattering measurements of the acoustic mode phonon dispersion relations¹³ of pyrope, the vibrational spectrum of hydrogarnets,¹⁴ and the phonon density of states of crystalline and glassy samples of grossular,¹⁵ (aimed at understanding the anomalies in heat capacity) have been reported. Theoretical calculations have been used to study the acoustic

mode phonon frequencies of pyrope¹³ and the crystal structure,^{16,17} elastic properties^{16,17} and mean-square atomic displacements¹⁸ of garnets. Calculations of the thermodynamic properties of garnets using models of the density of states (based on observed elastic properties and Raman and infrared frequencies), have also been reported.^{17,19}

The mineral almandine finds several important geological applications.^{20,21} The phase equilibria of multicomponent systems²² including almandine have been extensively used as geothermometers and geobarometers. Almandine is also known to exhibit interesting magnetic behavior at low temperatures. Magnetic susceptibility measurements²³ reveal antiferromagnetic ordering in synthetic almandine at 7.5 K. Low-temperature heat capacity measurements using adiabatic calorimetry also indicate a λ transition at 8.7 K attributed to magnetic ordering of the Fe^{2+} sublattice.

It is of interest to understand the stability of almandine under lower mantle conditions. Earlier, aluminous garnet phases were believed to be absent⁵ in the Earth's lower mantle (due to the phase transitions of garnets to silicate perovskite^{3–5} at high pressure). Recent observations of a new tetragonal almandine-pyrope phase as inclusions in lower-mantle diamonds,² has revived the interest in understanding the equation of state- and high-pressure behavior of almandine-pyrope garnets.

A major geophysical goal is to predict the thermodynamic properties and phase transitions of mantle-forming phases at the pressure and temperature they experience in the earth's interior. An essential prerequisite for these studies is an accurate understanding of the phonon density of states. In this paper, using a combination of theoretical lattice dynamical calculations and inelastic neutron-scattering studies, we have studied the phonon density of states and its manifestations in various thermodynamic properties of the garnet end-member almandine. The calculations enabled microscopic interpretations of the measured inelastic neutron-scattering data. The model has also been fruitfully used to compute various microscopic and macroscopic properties including the crystal structure, elastic constants, phonon frequencies, density of states, specific heat, thermal expansion, equation of state,

and mean square-atomic displacements of almandine; the results are overall in good agreement with the experimental data. The organization of the paper is as follows: Section II gives the experimental details, while Sec. III describes the lattice dynamical studies. A discussion of the results is given in Sec. IV, while Sec. V presents the conclusions.

II. EXPERIMENT

The natural polycrystalline sample of almandine is purified using chemical and magnetic analysis. Structural analysis from neutron powder diffraction indicates that the almandine sample is of a single phase. The inelastic neutron scattering experiments were carried out using the high-resolution medium-energy chopper spectrometer (HRMECS) at the Intense Pulsed Neutron Source of Argonne National Laboratory. The HRMECS spectrometer is based on the time-of-flight technique and is equipped with a large detector bank covering a wide range (-10° to 140°) of scattering angles. By choosing a relatively high incident neutron energy (E_o around 250 meV), measurement of the scattering function $S(Q, E)$ over a wide range of momentum and energy transfers can be undertaken and the data can be averaged over a wide range of Q from 10 to 15 \AA^{-1} . This procedure is needed to ensure an effectively uniform sampling of wavevectors over the Brillouin zone, according to the incoherent approximation.²⁴ In general, the energy resolution ΔE (full width at half-maximum) of HRMECS varies from $\sim 4\%$ of the incident energy (E_o) in the elastic region to $\sim 2\%$ near the end of the neutron energy-loss spectrum. A polycrystalline sample of 40 gm was placed inside a sealed aluminum container in the shape of a thin slab (dimension $75 \times 100 \times 2 \text{ mm}^3$), which was mounted on to the cold plate of a high-power closed-cycle helium refrigerator at a 45° angle with the incident neutron beam. Such a geometry minimized multiple scattering effects. In order to reduce multiphonon scattering, the phonon measurements were carried out at low temperatures (6 K and 15 K). The low-temperature specific heat¹¹ data and magnetic susceptibility measurements²³ show that there is an antiferromagnetic to paramagnetic transition at temperature around 7.5 K. We have carried out additional runs with $E_o = 40 \text{ meV}$ at small wave vectors ($Q < 4 \text{ \AA}^{-1}$), at 6 K and 15 K to separate the magnetic and phonon contributions. Background scattering was subtracted from the data by using an empty-container run. Measurements of elastic incoherent scattering from a vanadium standard provided detector calibration and intensity normalization.

The phonon density of states can be obtained from the measured scattering function $S(Q, E)$ which in the incoherent approximation is given by²⁴

$$S_{inc}^{(1)}(Q, E) = \sum_k \frac{b_k^2}{\langle b^2 \rangle} e^{-2W_k(Q)} \frac{Q^2}{2m_k} \frac{g_k(E/\hbar)}{E} (n+1), \quad (1)$$

where the population factor $n = [\exp(E/k_B T) - 1]^{-1}$, $2W_k$ is the Debye-Waller factor, and m_k and $g_k(\omega)$ are, respectively, the mass and displacement weighted density of states of atoms of type k .

Almandine

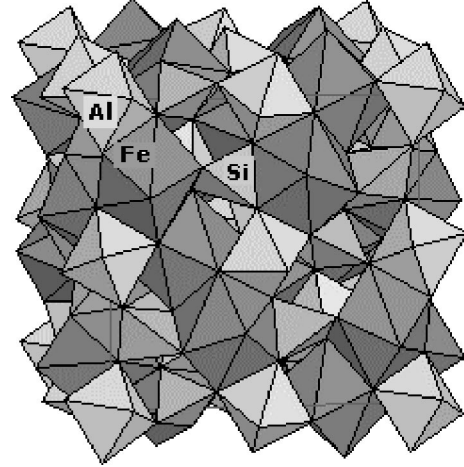


FIG. 1. Polyhedral representation of the structure of almandine, $\text{Fe}_3\text{Al}_2\text{Si}_3\text{O}_{12}$. The dodecahedra around Fe atoms, octahedra around Al atoms, and the silicate tetrahedra are shown.

III. LATTICE DYNAMICAL CALCULATIONS

The garnets crystallize in cubic system^{6,7} (space group $Ia\bar{3}d$). The body-centered cell contains eight formula units of $A_3B_2C_3O_{12}$, where A , B , and C ($=\text{Si}$ for silicate garnets) are cations. A , B , and Si cations forms three types of coordination polyhedra (Fig. 1) with O anions: a dodecahedron around A cation, an octahedron around B cation and a tetrahedra around Si . In view of the structural complexity which involves large number of atoms in the unit cell, we have carried out lattice dynamical studies using an atomistic approach involving semiempirical interatomic potentials.

The calculations have been carried in the quasiharmonic approximation using the interatomic potentials consisting of Coulombic and short ranged Born-Mayer type interactions terms, given by

$$V(r) = \frac{e^2}{4\pi\epsilon_0} \frac{Z(k)Z(k')}{r} + a \exp\left[\frac{-br}{R(k)+R(k')}\right] - \frac{C}{r^6}, \quad (2)$$

where, r is the separation between the atoms of a type k and k' and $R(k)$ and $Z(k)$ are, respectively, the effective radius and charge of the k th atom. $a = 1822 \text{ eV}$, $b = 12.364$, and $C = 100 \text{ eV \AA}^6$ have been treated as constants; this choice has been successfully used earlier to study the phonon density of states and thermodynamic properties of several complex solids.²⁵ The effective charge and radius parameters used in our calculations are given in Table I. The van der Waals interaction has been introduced only between the oxygen atoms. The stretching potential between Si-O bond is of the form

TABLE I. The potential parameters used in the shell model calculations.

| | Fe | Al | Si | O |
|----------------------|------|------|------|-------|
| Z | 1.66 | 2.31 | 2.40 | -1.40 |
| R (\AA) | 1.47 | 1.27 | 1.03 | 1.89 |

TABLE II. Comparison between the experimental (Ref. 6) (at 293 K) and calculated structural parameters (at 0 K). For the space group $Ia\bar{3}d$, the Fe, Al, Si, and O atoms are located at $(0,0.25,0.125)$, $(0,0,0)$, $(0.375,0,0.25)$, and (u, v, w) , respectively, and their symmetry equivalent positions.

| | Experimental | Calculated |
|-----------------|--------------|------------|
| $a(\text{\AA})$ | 11.523 | 11.5336 |
| u | 0.0340 | 0.0359 |
| v | 0.0490 | 0.0464 |
| w | 0.65278 | 0.6539 |

$$V(r) = -D \exp[-n(r-r_o)^2/(2r)], \quad (3)$$

where $D=2.3$ eV, $n=10.0 \text{ \AA}^{-1}$, $r_o=1.80 \text{ \AA}$. The polarizability of the oxygen atom has been introduced in the framework of the shell model^{25,26} with the shell charge $Y(O)=-2.0$ and shell-core force constant $K(O)=110 \text{ eV \AA}^{-2}$.

The calculated structure and elastic constants of almandine (Tables II and III) are in very good agreement with available experimental data. The calculations have been carried out using the current version of the software DISPR (Ref. 27) developed at Trombay.

The phonon density of states is calculated by integrating over a $4 \times 4 \times 4$ mesh of wave vectors in one octant of the cubic reciprocal space unit cell. The experimentally measured phonon density of states is weighted with the neutron-scattering cross-section of the constituent atoms. To compare with the experimental data, we have calculated the neutron-cross-section-weighted one phonon density of states, given by

$$g^{(n)}(E) = A \sum_k \frac{4\pi b_k^2}{M_k} g_k(E), \quad (4)$$

where A is the normalization constant and b_k , M_k and $g_k(E)$ are respectively, the neutron-scattering length, mass, and partial density of states of the k th atom. The factor $4\pi b_k^2/M_k$ for Fe, Al, Si, and O atoms are 0.201, 0.055, 0.077 and 0.265 barns/amu, respectively.

The calculated phonon density of states was used to evaluate the specific heat. The thermal expansion in the quasiharmonic approximation is given by

$$\alpha_V = \frac{1}{BV} \sum_i \Gamma_i C_{Vi}(T), \quad (5)$$

TABLE III. Comparison between the experimental [Ref. 9(a)] and calculated bulk modulus B and elastic constants C_{ij} in GPa units. Another experimental value of $B=175$ GPa has been reported in Ref. 9(b).

| Elastic constant | Experimental | Calculated |
|------------------|-----------------|------------|
| B | 180.1 ± 0.7 | 181.47 |
| C_{11} | 310.1 ± 1.6 | 317.68 |
| C_{44} | 92.9 ± 0.6 | 90.07 |
| C_{12} | 115.1 ± 0.7 | 113.37 |

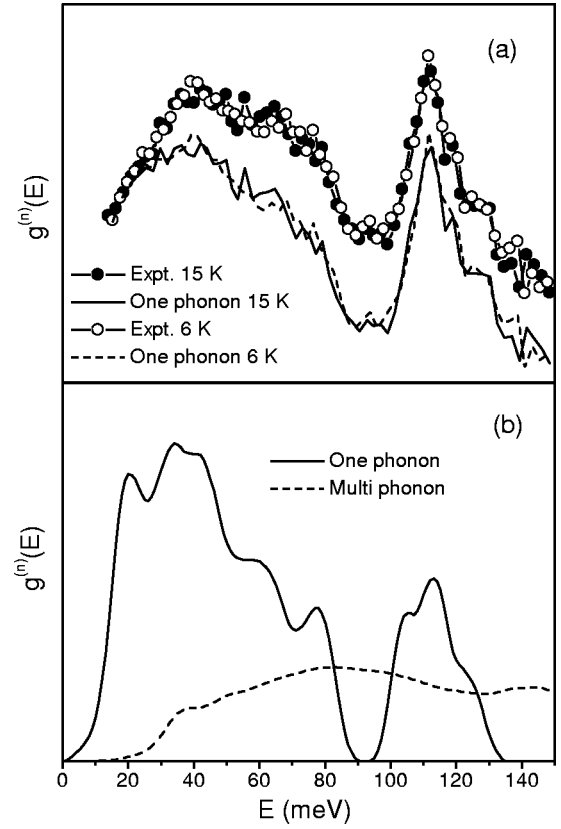


FIG. 2. (a) The experimental neutron-weighted phonon density of states at 6 K and 15 K (averaged over wave vector $Q=10-15 \text{ \AA}^{-1}$ for an incident neutron energy $E_o=250$ meV). The multiphonon contribution shown in (b) has been subtracted from experimental data to obtain the experimental one-phonon spectrum. (b) The calculated neutron-weighted one-phonon and multiphonon spectrum. The multiphonon spectrum is essentially the same at 6 K and 15 K. The calculated spectra have been convoluted with a Gaussian of FWHM of 8 meV in order to correspond to the energy resolution in the experiment (which varies from 2 to 4 % of the incident energy of 250 meV). The ordinate is in arbitrary units.

where Γ_i and $C_{Vi}(T)$ is the Gruneisen parameter and specific heat contribution from phonons in state i ($=\mathbf{q}j$, which refers to the j th phonon mode at wave vector \mathbf{q}) and B is bulk modulus. The volume thermal expansion is determined by integrating over the contribution of phonons of wave vectors on a $4 \times 4 \times 4$ mesh in an octant of the cubic Brillouin zone. The explicit anharmonic contributions to the thermal expansion (arising from the higher-order terms in the crystal potential) are also important and have been estimated using the formalism of Ref. 28.

IV. RESULTS AND DISCUSSION

The phonon density of states measurements in the energy range of 15–150 meV carried out at two temperature of 6 K and 15 K are shown in Fig. 2(a). The experimental one-phonon spectra are obtained by subtracting the multiphonon contribution from the experimental data. The multiphonon contribution is obtained using the Sjolander formalism.²⁹ The comparison between the experimental and calculated neutron-weighted one-phonon density of states (Fig. 2) shows that the measurements are in good agreement with the

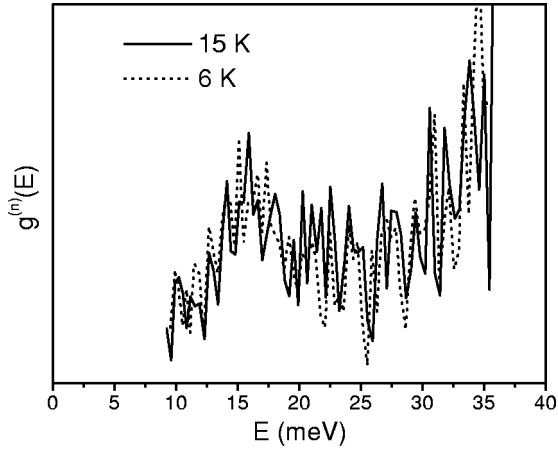


FIG. 3. The experimental neutron-weighted phonon density of states at small wave vectors ($Q < 4 \text{ \AA}^{-1}$) with incident neutron energy of 40 meV at 6 and 15 K. There is no significant difference between the data taken at these two temperatures. The ordinate is in arbitrary units.

calculations. The phonon spectrum consists of a broad phonon band centered about 40 meV and another band around 115 meV. There is a gap in the phonon density of states around 80 meV.

At small wave vectors ($Q < 4 \text{ \AA}^{-1}$) the observed spectra contain both nuclear scattering from atomic vibrations and magnetic scattering from the magnetic moments of the Fe ions. We have carried out additional runs with $E_o = 40$ meV at 6 and 15 K (Fig. 3). Above the Neel temperature (at 15 K), the magnetic contribution arises from paramagnetic scattering of the Fe ions, which constitute an isotropic background falling off in Q according to the square of the Fe^{2+} magnetic form factor. The observed spectra are dominated by a broad phonon peak centered at ~ 16 meV, which is in good agreement with the calculated phonon DOS (see Fig. 2). Below the Neel temperature (at 6 K) the magnetic contribution is characteristic of the magnon (spin waves) density of states. The spin-wave dispersion curves of almandine are not known. Theoretical calculations³⁰ of the magnon dispersion relations for the garnet $\text{Fe}_2\text{Ca}_3\text{Ge}_3\text{O}_{12}$ indicate that the magnon energies span the 0–2 meV range, which is outside that of the present measurement (15–150 meV). The observed spectra at 6 K indeed resemble that of 15 K with only a slight increase of background around 15 meV indicating that there is no magnetic scattering observed in our experiments.

The partial densities of states for different atoms in almandine, $\text{Fe}_3\text{Al}_2\text{Si}_3\text{O}_{12}$ are shown in Fig. 4. The Fe atoms mainly contribute in the 0–50 meV range, while the Al and Si atoms contribute in the 0–80 meV and the entire 0–140 meV ranges, respectively. Above 80 meV the contributions are mainly due to Si-O stretching modes. The partial densities of states are used for the calculation of the isotropic temperature factors for different atoms (Table IV) at 100 and 293 K. The calculated isotropic temperature factors are in fair agreement with the available experimental data.⁶

As the structure contain 80 atoms in the primitive cell, there are 240 phonon modes at the zone center, which are classified as follows:

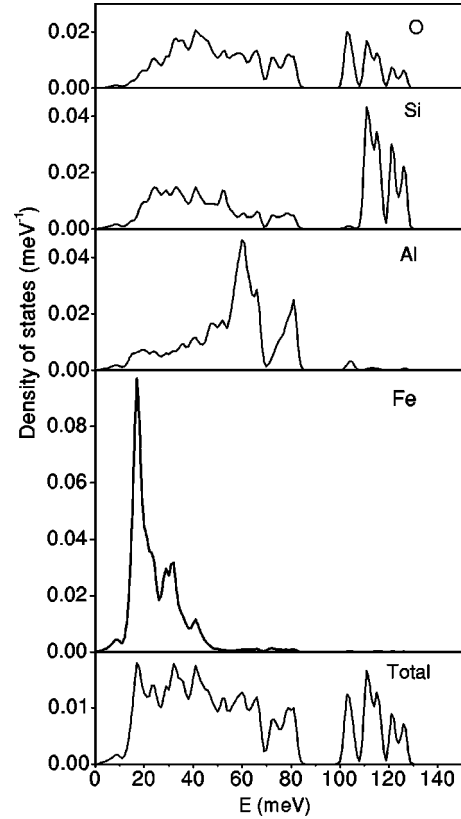


FIG. 4. The calculated partial density of states for different atoms and the total one-phonon density of states (all normalized to unity).

$$\Gamma: 3A_{1g} + 5A_{2g} + 8E_g + 14T_{1g} + 14T_{2g} + 5A_{1u} + 5A_{2u} + 10E_u \\ + 18T_{1u} + 16T_{2u}.$$

The T_{1g} , E_g , and A_{1g} modes are Raman active and T_{1u} are infrared active. There are large number of optically active modes, which have been observed in spectroscopic experiments⁸ in the range of 111 to 1038 cm^{-1} . This energy range compares very well with our calculated range of optic modes of 120 to 1026 cm^{-1} .

The calculated one-phonon density of states $g(E)$ is shown in Fig. 4, and is used to compute the specific heat $C_V(T)$ as a function of temperature. The anharmonic correction to the specific heat $C_p - C_V = \alpha_V^2 BVT$ is also calculated to obtain $C_p(T)$.³¹ The calculated specific heat $C_p(T)$ is compared with the experimental data in Fig. 5. The anharmonic corrections are about 3.0% at high temperature of 1500 K. The measured specific heat shows an anomaly at 7.5 K, which corresponds to the Neel temperature of almandine.

TABLE IV. Comparison between experimental (Ref. 6) and calculated isotropic temperature factors B_{iso} (\AA^2) at 100 and 293 K.

| | Experimental | | Calculated | |
|----|--------------|-------|------------|-------|
| | 100 K | 293 K | 100 K | 293 K |
| Fe | 0.215 | 0.462 | 0.195 | 0.453 |
| Al | 0.119 | 0.211 | 0.164 | 0.290 |
| Si | 0.107 | 0.172 | 0.150 | 0.277 |
| O | 0.221 | 0.344 | 0.252 | 0.429 |

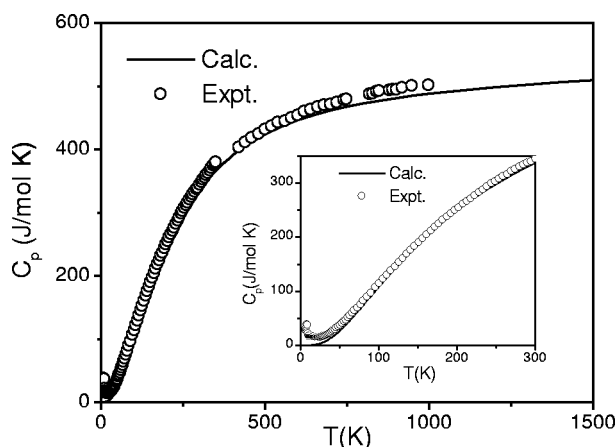


FIG. 5. The comparison between the calculated and experimental (Ref. 11) specific heat data. Inset shows the comparison between the calculation and experiment below 300 K.

Our calculation of specific heat does not include the contributions arising from the spin waves. The experimental value of C_p is higher than the calculated phonon contribution below 50 K. Above 50 K the calculated and experimental data are in good agreement. The calculated Debye temperature varies from 510 K at 4 K to 590 K at 1500 K. The percentage relative volume expansion [Fig. 6(a)] calculated in quasiharmonic and anharmonic approximations are in overall good agreement with the available experimental data.³² So also, the calculated equation of state [Fig. 6(b)] is in very good agreement with the experiments.⁹

V. CONCLUSIONS

This paper reports detailed lattice dynamical studies including inelastic neutron-scattering measurements and shell model calculations of the phonon density of states and thermodynamic properties of the garnet mineral, almandine. The model agrees very well with the neutron and thermodynamic data. The calculations have enabled a microscopic interpretation of the experimental inelastic neutron-scattering data. The calculated structure, elastic constants, phonon frequencies, specific heat, thermal expansion, equation of state, and mean-square atomic displacements are also found to be in good agreement with the experimental data. The interatomic potentials developed in these studies may be used to study the structural, vibrational, and thermodynamic properties of the other garnet minerals, which may eventually lead to an understanding of the mixing properties of garnets.

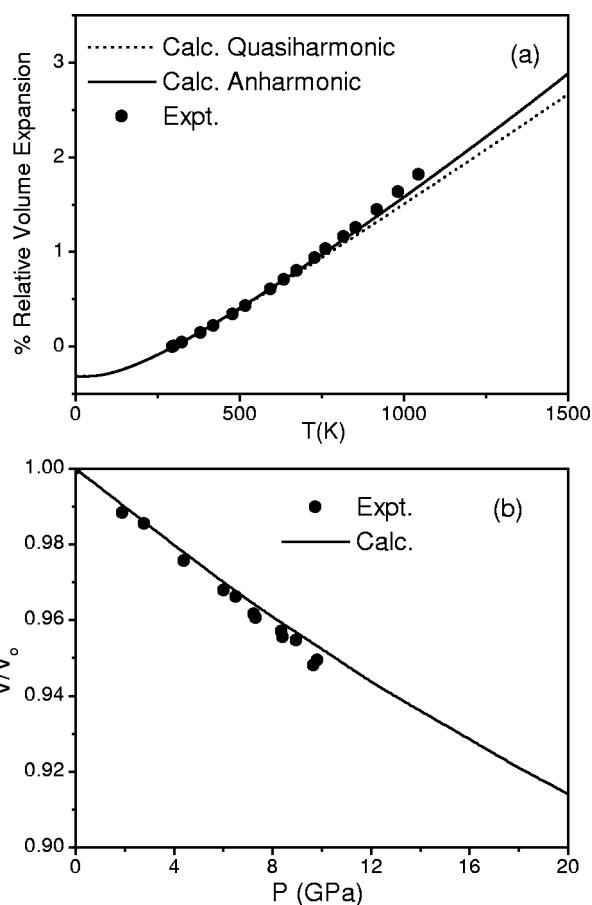


FIG. 6. (a) Comparison between the calculated and experimental data (Ref. 32) of cell volumes at different temperatures [$(V_T/V_{298} - 1) \times 100\%$, V_T and V_{298} being the cell volumes at temperatures T and 298 K respectively]. (b) Comparison between the calculated and experimental [Ref. 9(b)] equation of state. V_0 and V are the cell volumes at ambient pressure and pressure P , respectively.

ACKNOWLEDGMENTS

The natural sample of almandine was provided by Dr. K. K. Sharma, Wadia Institute of Himalayan Geology, Dehra Dun, India. We also acknowledge assistance from Dr. N. Krishna Rao and his colleagues at the Ore Dressing Section, BARC, Hyderabad, India while purifying the natural polycrystalline sample of almandine. Work performed at Argonne National Laboratory was supported by the U.S. DOE-BES under Contract No. W-31-109-ENG-38.

¹W. Prandl and Th. Bruckl, in *Advances in Physical Geochemistry, Structural and Magnetic Phase Transitions in Minerals*, edited by S. Ghose, J.M.D. Coey, and E. Salje (Springer-Verlag, New York, 1988), Vol. 7, p. 208; *Physics of Magnetic Garnets*, Proceedings of the International School of Physics "Enrico Fermi," Course LXX, edited by A. Paoletti (North-Holland, Amsterdam, 1978); G.A. Novak and G.V. Gibbs, *Am. Mineral.* **56**, 791 (1971); E.P. Meagher, in *Rev. in Mineralogy, Orthosilicates*, edited by P.H. Ribbe (Mineralogical Society of America, Wash-

ington D.C., 1980), Vol. 5, p. 25.

²J. Harris, M.T. Hutchison, M. Hursthouse, M. Light, and B. Harte, *Nature (London)* **387**, 486 (1997); C. McCammon, M. Hutchison, and J. Harris, *Science* **278**, 434 (1997).

³N. Funamori, T. Yagi, N. Miyajima, and K. Fujino, *Science* **275**, 513 (1997).

⁴T. Kato and M. Kumazawa, *Nature (London)* **316**, 803 (1985).

⁵T. Irifune, *Nature (London)* **370**, 131 (1994).

⁶T. Armbruster, C.A. Geiger, and G.A. Lager, *Am. Mineral.* **77**,

- 512 (1992); C.A. Geiger, T. Armbruster, G.A. Lager, K. Jiang, W. Lottermoser, and G. Amthauer, *Phys. Chem. Miner.* **19**, 121 (1992).
- ⁷A. Pavese, G. Artioli, and M. Prencipe, *Am. Mineral.* **80**, 457 (1995); L. Zhang, H. Ahsbaks, and A. Kutoglu, *Phys. Chem. Miner.* **25**, 301 (1998); T. Arlt, T. Armbruster, R. Miletich, P. Ulmer, and T. Peters, *ibid.* **26**, 100 (1998).
- ⁸A.M. Hofmeister and A. Chopelas, *Phys. Chem. Miner.* **17**, 503 (1991); *Am. Mineral.* **81**, 418 (1996); B.A. Kolesov and C.A. Geiger, *Phys. Chem. Miner.* **25**, 142 (1998).
- ⁹(a) D.G. Isaak and E.K. Graham, *J. Geophys. Res.* **81**, 2483 (1976); (b) Y. Sato, M. Akogi, and S. Akimoto, *ibid.* **83**, 335 (1978); (c) M. Chai, J.M. Brown, and L. Slutsky, *Geophys. Res. Lett.* **24**, 523 (1997); (d) G. Chen, H.A. Spertzler, I.C. Getting, and A. Yoneda, *ibid.* **23**, 5 (1996).
- ¹⁰O' Neill, J.D. Bass, J.R. Smyth, and M.T. Vangham, *J. Geophys. Res.* **94**, 17 819 (1989); O' Neill, J.D. Bass, G.R. Rossman, C.A. Geiger, and K. Langer, *Phys. Chem. Miner.* **17**, 617 (1991); P.G. Conrad, C.S. Zha, H.K. Mao, and R.J. Hemley, *Am. Mineral.* **99**, 374 (1999).
- ¹¹L.M. Anovitz, E.J. Essene, G.W. Metz, S.R. Bohlen, E.F. Westrum, Jr., and B.S. Hemingway, *Geochim. Cosmochim. Acta* **57**, 4191 (1993).
- ¹²L. Thieblot, C. Tequi, and P. Richet, *Am. Mineral.* **84**, 848 (1999); C.A. Geiger and T. Armbruster, *ibid.* **82**, 740 (1997).
- ¹³G. Artioli, A. Pavese, and O. Moze, *Am. Mineral.* **81**, 19 (1996).
- ¹⁴G.A. Lager, J.C. Nipko, and C.-K. Loong, *Physica B* **241-243**, 406 (1998).
- ¹⁵J. Zhao, P.H. Gaskell, L. Cormier, and S.M. Bennington, *Physica B* **241**, 906 (1998).
- ¹⁶M. Matsui, *Phys. Chem. Miner.* **23**, 345 (1996).
- ¹⁷G. Ottonello M. Molereta, and P.F. Scinto, *Am. Mineral.* **81**, 429 (1996).
- ¹⁸T. Pilati, F. Demartin, and C.M. Gramaccioli, *Acta Crystallogr., Sect. B: Struct. Sci.* **B52**, 239 (1996).
- ¹⁹A.M. Hofmeister and A. Chopelas, *Am. Mineral.* **76**, 880 (1991).
- ²⁰The appearance of almandine rich garnets has been used as an indicator of physical metamorphism [Ref. 21(a)]. Garnets including almandine have also been used for dating of rocks [Ref. 21(b)].
- ²¹(a) G. Barrow, *Geol. Soc. London Quart. J.* **49**, 330 (1983); (b) S. Duchene, J. Blichert, B. Luais, and P. Telouk, *Nature (London)* **387**, 586 (1997).
- ²²L.Y. Arnovich and R.G. Berman, *Am. Mineral.* **82**, 345 (1997); J.M. Ferry and F.S. Spear, *Contrib. Mineral. Petrol.* **66**, 113 (1978); D.J. Ellis and D.H. Green, *ibid.* **71**, 13 (1979); S.T.C. O'Neill and B.J. Wood, *ibid.* **70**, 59 (1979); S.R. Bohlen, V.J. Wall, and A.L. Boettcher, *Am. Mineral.* **68**, 1049 (1983); S.R. Bohlen, W.A. Dollase, and V.J. Wall, *J. Petrol.* **27**, 1143 (1986).
- ²³W. Prandl, *Z. Kristallogr.* **134**, 334 (1971).
- ²⁴D.L. Price and K. Skold, in *Neutron Scattering*, edited by K. Skold and D.L. Price (Academic Press, Orlando, 1986), Vol. A; J.M. Carpenter and D.L. Price, *Phys. Rev. Lett.* **54**, 441 (1985); S.N. Taraskin and S.R. Elliott, *Phys. Rev. B* **55**, 117 (1997).
- ²⁵R. Mittal and S.L. Chaplot, *Phys. Rev. B* **60**, 7234 (1999).
- ²⁶P. Bruesch, in *Phonons: Theory and Experiments* (Springer, Berlin, 1982), Vol. 1.
- ²⁷S.L. Chaplot (unpublished).
- ²⁸V.K. Jindal and J. Kalus, *Phys. Status Solidi B* **133**, 89 (1986); R. Bhandari and V.K. Jindal, *J. Phys.: Condens. Matter* **3**, 899 (1991).
- ²⁹A. Sjolander, *Ark. Fys.* **14**, 7435 (1988).
- ³⁰Th. Bruckl and W. Prandl, *Z. Phys. B: Condens. Matter* **73**, 57 (1988).
- ³¹N. Choudhury, S.L. Chaplot, and K.R. Rao, *Phys. Chem. Miner.* **16**, 599 (1989).
- ³²B.J. Skinner, *Am. Mineral.* **41**, 428 (1956).